Available online at www.sciencedirect.com
SCIENCE DIRECT
C. R. Geoscience 338 (2006) 420–432
COMPTES RENDUS GEOSCIENCE
http://france.elsevier.com/direct/CRAS2A/

Geomaterials (Mineralogy)

Green rusts synthesis by coprecipitation of Fe^{II}–Fe^{III} ions and mass-balance diagram

Christian Ruby *, Rabha Aïssa, Antoine Géhin, Jérôme Cortot, Mustapha Abdelmoula, Jean-Marie Génin

Laboratoire de chimie physique et microbiologie pour l'environnement, UMR 7564 CNRS, université Henri-Poincaré–Nancy-1, équipe 'Microbiologie et Physique' & Département 'Matériaux et Structures', ESSTIN, 405, rue de Vandœuvre, 54600 Villers-lès-Nancy, France

Received 17 January 2005; accepted after revision 13 April 2006

Written on invitation of the Editorial Board

Abstract

A basic solution is progressively added to various mixed Fe^{II}–Fe^{III} solutions. The nature and the relative quantities of the compounds that form can be visualised in a mass-balance diagram. The formation of hydroxysulphate green rust $\{GR(SO_4^{2-})\}$ is preceded by the precipitation of a sulphated ferric basic salt that transforms in a badly ordered ferric oxyhydroxide. Then octahedrally coordinated Fe^{II} species and SO_4^{2-} anions are adsorbed on the FeOOH surface and $GR(SO_4^{2-})$ is formed at the solid/solution interface. By using the same method of preparation, other types of green rust were synthesised, e.g. hydroxycarbonate green rust $\{GR(CO_3^{2-})\}$. Like other layered double hydroxides, green rusts obey the general chemical formula $[M^{II}_{(1-x)}M^{III}_x(OH)_2]^{x-}\cdot[(x/n)\,A^{n-}\cdot m\,H_2O]^{x+}$ with $x \leqslant 1/3$. Al-substituted hydroxysulphate green rust consists of small hexagonal crystals with a lateral size ∼50 nm, which is significantly smaller than the size of the $GR(SO_4^{2-})$ crystals (∼500 nm). ***To cite this article: C. Ruby et al., C. R. Geoscience 338 (2006).***

Résumé

Synthèse des rouilles vertes par coprécipitation d'ions Fe^{II} et Fe^{III} et diagramme bilan matière. Une solution basique est introduite progressivement dans différentes solutions mixtes Fe^{II}–Fe^{III}. La nature et les quantités relatives de chaque composé sont visualisées dans un diagramme bilan-matière. La formation de la rouille verte sulfatée $\{RV(SO_4^{2-})\}$ est précédée par la précipitation d'un sel basique ferrique sulfaté, qui se transforme en un oxyhydroxide ferrique mal cristallisé. Ensuite, des cations Fe^{II} en coordinence octaédrique et des anions sulfates sont adsorbés à la surface de l'oxyhydroxide ferrique et $RV(SO_4^{2-})$ se forme à l'interface solide/solution. Comme d'autres hydroxydes doubles lamellaires, les rouilles vertes obéissent à la formule chimique $[M^{II}_{(1-x)}M^{III}_x(OH)_2]^{x-}\cdot[(x/n)\,A^{n-}\cdot m\,H_2O]^{x+}$, avec $x \leqslant 1/3$. La rouille verte sulfatée substituée aluminium est caractérisée par des cristaux de forme hexagonale dont la taille (∼50 nm) est beaucoup plus faible que celle des cristaux de $RV(SO_4^{2-})$ ∼500 nm. ***Pour citer cet article : C. Ruby et al., C. R. Geoscience 338 (2006).***

* Corresponding author.
E-mail address: ruby@lcpe.cnrs-nancy.fr (C. Ruby).

1631-0713/$ – see front matter
doi:10.1016/j.crte.2006.04.008

Keywords: Iron; Aluminium; Green Rust; Coprecipitation; Mössbauer

Mots-clés : Fer ; Aluminium ; Rouille Verte ; Coprécipitation ; Mössbauer

1. Introduction

In soils, Fe^{III} species are very frequently trapped in solid iron oxyhydroxides. In contrast, Fe^{II} species move much more rapidly because they are easily dissolved. Therefore, the understanding of the possible chemical reactions that occur at the solid/solution interface between Fe^{II} dissolved species and the various ferric oxyhydroxides is fundamental. It is now well established that dissimilatory iron reducing bacteria (DIRB) play a major role in the biogeochemical cycle of iron, because they are responsible for the reductive dissolution of ferric oxyhydroxides FeOOH. Once Fe^{II} dissolved species are produced by the bacteria, a reaction of coprecipitation between Fe^{II} species and the Fe^{III} species remaining into FeOOH may occur and mixed Fe^{II}–Fe^{III} compounds form. Such coprecipitation reactions between Fe^{II} and Fe^{III} species were studied in abiotic conditions by several authors, e.g., [2,8,9,12,15–17]. It was namely shown that Fe^{II} species react easily with lepidocrocite (or ferrihydrite) to form either green rust [8,16] or magnetite [9,12,17] and that the adsorption of hydroxylated Fe^{II} species on the surface of the ferric oxyhydroxide FeOOH was an initial step that precedes the formation of magnetite [15,17]. In Fe^{III} rich medium, the formation of magnetite Fe_3O_4 was favoured, but was sometimes preceded by the precipitation of green rusts [12,15]. It is now well established that in anoxic conditions green rusts are transformed either in a mixture of magnetite and siderite $\{Fe_3O_4, FeCO_3\}$, when carbonate anions are present [3,5], or in a mixture of magnetite and ferrous hydroxide $\{Fe_3O_4, Fe(OH)_2\}$ [14] at pH higher than 9.

By using the experimental method used in the early work of Arden [2], reactions of coprecipitation were studied systematically by performing the titration of various Fe^{II}–Fe^{III} solutions [14]. A mass-balance diagram was shown to be a powerful tool to study the various steps of the reaction and the properties of this diagram are explained here. The formation of hydroxycarbonate green rust and Al-substituted hydroxysulphate green rust by coprecipitation was also studied recently [1,5].

2. Experimental method

The samples were prepared by the coprecipitation of Fe^{II} and Fe^{III} species in different kinds of aqueous solutions. This simple method, which consists to add a basic solution to a mixture that contains Fe^{II} and Fe^{III} dissolved species, is well known for the synthesis of the other members of the layered double hydroxides (LDHs) family. Due to the fact that the divalent cation Fe^{II} can easily be oxidised, the evacuation of dissolved oxygen was ensured by a continuous N_2 bubbling in the aqueous solution introduced in a gas tight reactor. The initial solution was prepared by dissolving in demineralised water appropriate amounts of Fe^{II} and Fe^{III} salts. A basic solution was progressively added to the initial mixture by using a peristaltic pump at a constant flow rate of $\sim$0.5 ml min^{-1}. The duration of the experiments was $\sim$5 h and the pH of the solution was monitored continuously. Depending on the type of samples that was synthesised, different methods were used that are summarised in Table 1. The suspensions were filtered under an inert atmosphere and the precipitates were analysed by several techniques: X-ray diffraction (XRD) at a wavelength $\lambda(\mathrm{Co\,K}\alpha_1) = 0.1789$ nm, transmission Mössbauer spectroscopy (TMS) and transmission electron microscopy (TEM). Details concerning the method of analyses were given in a previous work [14]. The Mössbauer spectra were calibrated by using an iron foil at room temperature and were fitted with Lorentzian-shape lines. The concentrations of Fe and SO_4^{2-} in the aqueous solution were measured by inductively coupled plasma-atomic emission spectroscopy (ICP-AES). Titration with 1,10-phenantroline was used for ferrous iron determination.

3. Properties of the mass-balance diagram

3.1. Construction of the diagram

If one considers the mass-balance of the previously described coprecipitation experiments, the nature and the relative abundances of the iron containing compounds that form are governed by two parameters: (*i*) the ferric molar fraction of the initial mixed Fe^{II}–Fe^{III} solution, i.e. the ratio $x = n(Fe^{III})/[n(Fe^{II}) + n(Fe^{III})]$; (*ii*) the hydroxylation rate that corresponds to the molar ratio $R = n(OH^-)/[n(Fe^{II}) + n(Fe^{III})]$ where $n(OH^-)$ represents the number of moles of hydroxyl species added in solution, $n(Fe^{III})$ and $n(Fe^{II})$ are the numbers of Fe^{III} and Fe^{II} ions introduced into the initial solution. The value of the ratio R is well defined when

Table 1
Conditions of preparation of the samples synthesised by coprecipitation: hydroxysulphate green rust {$GR(SO_4^{2-})$}, hydroxycarbonate green rust {$GR(CO_3^{2-})$} and Al-substituted hydroxysulphate green rust {Al-$GR(SO_4^{2-})$}

Tableau 1
Conditions de préparation des échantillons synthétisés par coprécipitation : rouille verte sulfatée {$GR(SO_4^{2-})$}, rouille verte carbonatée {$GR(CO_3^{2-})$} et rouille verte sulfatée substituée aluminium {Al-$GR(SO_4^{2-})$}

Type of green rust	$x = n(Fe^{III})/n_{tot}$	$x(Al^{III}) = n(Al^{III})/n_{tot}$	Salts and concentration of the initial solution	Base
$GR(SO_4^{2-})$	0 ; 0.1 ; 0.14 ; 0.17 ; 0.2 ; 0.25, 0.33 ; 0.5 ; 0.67, 1	0	$FeSO_4{\cdot}7\,H_2O$ $Fe_2(SO_4)_3{\cdot}5\,H_2O$ $[Fe] = 4 \times 10^{-1}$ M	$[NaOH] = 0.8$ M
$GR(CO_3^{2-})$	0, 0.33, 0.4, 0.5, 1	0	$FeSO_4{\cdot}7\,H_2O$ $Fe_2(SO_4)_3{\cdot}5\,H_2O$ $[Fe] = 6.7 \times 10^{-2}$ M	$[Na_2CO_3] = 0.57$ M
$GR(CO_3^{2-})$	0.25	0	$FeCl_2{\cdot}4\,H_2O$ $FeCl_3{\cdot}6\,H_2O$ $[Fe] = 6.7 \times 10^{-2}$ M	$[Na_2CO_3] = 0.57$ M
Al-$GR(SO_4^{2-})$	0.2 ; 0.185 ; 0.16 ; 0.1	0 ; 0.015 ; 0.04 ; 0.1	$FeSO_4{\cdot}7\,H_2O$ $Fe_2(SO_4)_3{\cdot}5\,H_2O$ $Al_2(SO_4)_3{\cdot}5\,H_2O$ $[Fe]+[Al] = 4\times10^{-1}$ M	$[NaOH] = 0.8$ M

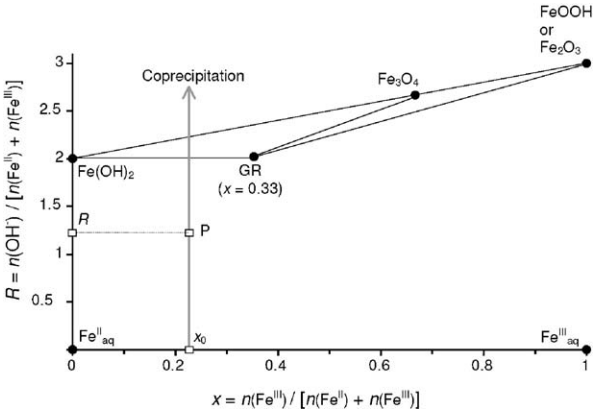

Fig. 1. Fe^{II}–Fe^{III} mass-balance diagram, showing the route of a coprecipitation experiment.

Fig. 1. Diagramme bilan matière du système Fe^{II}–Fe^{III} et représentation du chemin correspondant à une réaction de coprécipitation.

the basic solution used in the experiment is a strong base such as NaOH.

It is convenient to represent in a mass-balance diagram [14] the ratio $R = n(OH^-)/[n(Fe^{II}) + n(Fe^{III})]$ as a function of the ferric molar fraction $x = n(Fe^{III})/[n(Fe^{II}) + n(Fe^{III})]$ of the various iron species that may form (Fig. 1), where $n(OH^-)$, $n(Fe^{III})$ and $n(Fe^{II})$ represent here the number moles of OH^-, Fe^{III} and Fe^{II} consumed during the precipitation of 1 mol of iron of a given compound. As an example, the ferric oxyhydroxides of chemical formula FeOOH (or the ferric oxides Fe_2O_3) are represented by point $(1, 3)$ in the diagram presented in Fig. 1, because the precipitation of 1 mol of Fe^{III} into these compounds is described by the following chemical reactions:

$$Fe^{III}{}_{aq} + 3\,OH^- \Leftrightarrow FeOOH + H_2O, \quad (1a)$$

$$Fe^{III}{}_{aq} + 3\,OH^- \Leftrightarrow 1/2\,Fe_2O_3 + 3/2\,H_2O \quad (1b)$$

In a same manner, the position of the different solid compounds can easily be determined: ferrous hydroxide $Fe(OH)_2$, green rust (GR) of general chemical formula $[Fe^{II}{}_{(1-x)}Fe^{III}{}_x(OH)_2]^{x+}{\cdot}[(x/n)A^{n-}{\cdot}m\,H_2O]^{x-}$, magnetite Fe_3O_4 and ferric oxide Fe_2O_3 correspond respectively to points $(0, 2)$, $(x, 2)$, $(2/3, 8/3)$ and $(1, 3)$ (Fig. 1). Non-stoichiometric magnetite $Fe_{(3-x)}O_4$ is situated on the tie-line that links point $(2/3, 8/3)$ to point $(1, 3)$. The aqueous species $Fe^{II}{}_{aq}$ and $Fe^{III}{}_{aq}$ are represented by points $(0, 0)$ and $(0, 1)$, respectively.

3.2. Interpreting the diagram

A coprecipitation experiment that is realised at a constant ferric molar fraction ratio x_0 corresponds to the vertical line $x = x_0$ shown in Fig. 1. At each instant of the experiment, i.e. for each point $P(x_0, R)$ situated on the vertical line, the nature and the relative abundance of the different compounds that may precipitate can be determined graphically. Therefore, the following cases will be considered:

– (a) a single compound forms if P is situated at a point (x, R) that corresponds to a given com-

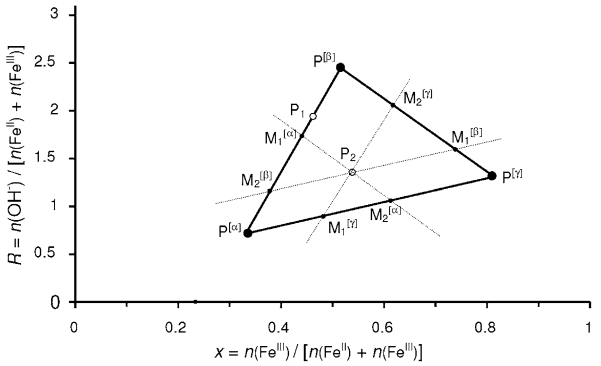

Fig. 2. Graphical determination of the relative abundance of the compounds in the mass-balance diagram. For point P_1, the two-compound system $\{\alpha+\beta\}$ forms and the relative quantities are given by Eqs. (7) and (8). For point P_2, the three-compound system $\{\alpha+\beta+\gamma\}$ forms and the relative quantities are given by Eqs. (12), (13) and (14).

Fig. 2. Détermination graphique des abondances relatives de chaque phase dans le diagramme bilan matière. Pour le point P_1, le système biphasé $\{\alpha+\beta\}$ se forme et les quantités relatives de chaque phase sont données par les Éqs. (7) et (8). Pour le point P_2, le système triphasé $\{\alpha+\beta+\gamma\}$ se forme et les quantités relatives de chaque phase sont données par les Éqs. (12), (13) et (14).

pound, e.g., point (0.33, 2) that corresponds to GR in Fig. 1;

– (b) a two-compound system forms if point P is situated on a tie-line that joins two compounds, e.g., the tie-line that joins $Fe(OH)_2$ to GR in Fig. 1. In a general case, let us consider the formation of a mixture of two compounds α and β that correspond to the two points $P^{[\alpha]}(x^{[\alpha]}, R^{[\alpha]})$ and $P^{[\beta]}(x^{[\beta]}, R^{[\beta]})$ presented in Fig. 2. The conservation of matter leads to:

$$n(OH^-) = n(OH^-)^{[\alpha]} + n(OH^-)^{[\beta]} \quad (2)$$

$$n(Fe^{III}) = n(Fe^{III})^{[\alpha]} + n(Fe^{III})^{[\beta]} \quad (3)$$

where $n(OH^-)$, $n(Fe^{III})$, $n(OH^-)^{[\alpha]}$, $n(Fe^{III})^{[\alpha]}$, $n(OH^-)^{[\beta]}$ and $n(Fe^{III})^{[\beta]}$ are the respective mole numbers of OH^- and Fe^{III} consumed during the formation of the whole mixture and their repartition in the α and β compounds. It can be demonstrated that Eqs. (2) and (3) are equivalent to the following equations:

$$R = n(OH^-)/n = (X^{[\alpha]} \cdot R^{[\alpha]}) + (X^{[\beta]} \cdot R^{[\beta]}) \quad (4)$$

$$x = n(Fe^{III})/n = (X^{[\alpha]} \cdot x^{[\alpha]}) + (X^{[\beta]} \cdot x^{[\beta]}) \quad (5)$$

$$\text{with } X^{[\alpha]} = (n^{[\alpha]}/n) \text{ and } X^{[\beta]} = (n^{[\beta]}/n)$$

Here n, $n^{[\alpha]}$ and $n^{[\beta]}$ are the total number of moles of iron in the whole mixture and their repartition in the α and β compounds. Therefore, $X^{[\alpha]}$ and $X^{[\beta]}$ are the relative amounts of Fe in α and β compounds, respectively. Eqs. (4) and (5) are equivalent to the following vectorial relation:

$$\mathbf{OP}_1 = X^{[\alpha]}\mathbf{OP}^{[\alpha]} + X^{[\beta]}\mathbf{OP}^{[\beta]} \quad (6)$$

So, the mixture $\{\alpha+\beta\}$ is indeed represented by a point P_1 situated on a tie-line that joins $P^{[\alpha]}$ to $P^{[\beta]}$ (Fig. 2). For given values of the Fe^{III} molar fractions x, $x^{[\alpha]}$, and $x^{[\beta]}$, the values of $X^{[\alpha]}$ and $X^{[\beta]}$ are determined by the well-known lever rule:

$$X^{[\alpha]} = (x^{[\beta]} - x)/(x^{[\beta]} - x^{[\alpha]}) = \left|\mathbf{P}_1\mathbf{P}^{[\beta]}\right| / \left|\mathbf{P}^{[\alpha]}\mathbf{P}^{[\beta]}\right| \quad (7)$$

$$X^{[\beta]} = (x - x^{[\alpha]})/(x^{[\beta]} - x^{[\alpha]}) = \left|\mathbf{P}^{[\alpha]}\mathbf{P}_1\right| / \left|\mathbf{P}^{[\alpha]}\mathbf{P}^{[\beta]}\right| \quad (8)$$

It should be noted that if Mössbauer spectroscopy is performed for analysing the $\{\alpha+\beta\}$ mixture, $X^{[\alpha]}$ and $X^{[\beta]}$ occur to be the relative areas of the subspectra of phases α and β, respectively. The quantitative predictions made with the mass-balance diagram can be directly compared to quantitative analyses made with Mössbauer spectroscopy as already done in a previous work [16];

– (c) a three-compound mixture forms if point P is situated inside a triangle of three compounds, e.g., $Fe(OH)_2$, GR and Fe_3O_4 in Fig. 1. Let us again consider the general case of three compounds represented by the three points $P^{[\alpha]}(x^{[\alpha]}, R^{[\alpha]})$, $P^{[\beta]}(x^{[\beta]}, R^{[\beta]})$ and $P^{[\gamma]}(x^{[\gamma]}, R^{[\gamma]})$ in Fig. 2. A similar demonstration to that followed for the two-compounds mixture will lead to the vectorial relation:

$$\mathbf{OP}_2 = X^{[\alpha]}\mathbf{OP}^{[\alpha]} + X^{[\beta]}\mathbf{OP}^{[\beta]} + X^{[\gamma]}\mathbf{OP}^{[\gamma]} \quad (9)$$

Point P_2 corresponds to the 3-phase system $\{\alpha+\beta+\gamma\}$. $X^{[\alpha]}$, $X^{[\beta]}$, and $X^{[\gamma]}$ are the relative amounts of Fe in phases α, β, and γ. According to Eq. (9) and to the constraint $X^{[\alpha]} + X^{[\beta]} + X^{[\gamma]} = 1$, P_2 is a barycentre of points $P^{[\alpha]}$, $P^{[\beta]}$ and $P^{[\gamma]}$ that lies inside triangle ($P^{[\alpha]}$, $P^{[\beta]}$, $P^{[\gamma]}$) of Fig. 2. If $P^{[\alpha]}$ or $P^{[\beta]}$ is chosen as an origin in the vectorial Eq. (9), one obtains the following equations:

$$\mathbf{P}^{[\alpha]}\mathbf{P}_2 = X^{[\beta]}\mathbf{P}^{[\alpha]}\mathbf{P}^{[\beta]} + X^{[\gamma]}\mathbf{P}^{[\alpha]}\mathbf{P}^{[\gamma]} \quad (10)$$

$$\mathbf{P}^{[\beta]}\mathbf{P}_2 = X^{[\alpha]}\mathbf{P}^{[\beta]}\mathbf{P}^{[\alpha]} + X^{[\gamma]}\mathbf{P}^{[\beta]}\mathbf{P}^{[\gamma]} \quad (11)$$

The Fe molar fractions $X^{[\alpha]}$, $X^{[\beta]}$ and $X^{[\gamma]}$ can be determined graphically by using the parallel to the sides of triangle ($P^{[\alpha]}$, $P^{[\beta]}$, $P^{[\gamma]}$) as shown in Fig. 2

and the following equations are verified:

$$X^{[\alpha]} = \left|M_1^{[\alpha]}P^{[\beta]}\right| / \left|P^{[\alpha]}P^{[\beta]}\right| = \left|M_2^{[\alpha]}P^{[\gamma]}\right| / \left|P^{[\alpha]}P^{[\gamma]}\right| \quad (12)$$

$$X^{[\beta]} = \left|M_1^{[\beta]}P^{[\gamma]}\right| / \left|P^{[\beta]}P^{[\gamma]}\right| = \left|M_2^{[\beta]}P^{[\alpha]}\right| / \left|P^{[\beta]}P^{[\alpha]}\right| \quad (13)$$

$$X^{[\gamma]} = \left|M_1^{[\gamma]}P^{[\alpha]}\right| / \left|P^{[\gamma]}P^{[\alpha]}\right| = \left|M_2^{[\gamma]}P^{[\beta]}\right| / \left|P^{[\gamma]}P^{[\beta]}\right| \quad (14)$$

4. Mechanism of formation of hydroxysulphate green rust

4.1. Analyses of the pH curves

For 10 different values of the ferric molar fraction x, titration curves were presented in a previous work [14] and three typical curves are shown in Fig. 3. The curves are characterised by three plateaus separated by two equivalent points E_1 and E_2. For $x \leqslant 0.2$, a slow down of the pH curves is observed around a critical point called E^* and the jump of pH is always preceded by a small peak between $R \sim 1.7$ and 1.95. A direct visualisation of the compounds that form during the titration is presented in Fig. 4 where the R values that correspond to equivalent points E_1, E_2 and E^* are indicated in the mass-balance diagram. One observes that the (x, R_1) values of points E_1 are situated on a line $R = \sim 2.75\,x$. This indicates that the compound that forms during the first plateau is a sulphated ferric basic salt, i.e. a ferric oxyhydroxide where some of the OH^- anions are substituted by SO_4^{2-} anions. Schwertmanite of general chemical formula $Fe_{16}O_{16}(OH)_y(SO_4)_z \cdot n\,H_2O$ ($16 - y = 2z$ and $2 \leqslant z \leqslant 3.5$) [4], which is also presented in the mass-balance diagram, is an example of such a ferric basic salt. When $x \leqslant 0.2$, the (x, R_2) values of points E_2 follow the line $R = 2$ of the binary system $\{Fe(OH)_2, GR(SO_4)\}$. For $0.25 \leqslant x \leqslant 0.67$, the points are situated in the triangle of the three-compound system $\{Fe(OH)_2, GR(SO_4^{2-}), Fe_3O_4\}$. The formation of these compounds was confirmed by using Mössbauer spectroscopy and the TMS spectra of two samples taken at points E_2 of the titration curves are given in Fig. 5a and b. Hyperfine parameters and quantitative predictions made with the mass-balance diagram are given in Table 2. At $T = 12$ K, the Mössbauer spectrum of $GR(SO_4^{2-})$ is easily distinguished from the spectrum of $Fe(OH)_2$, which is characterised by an octet, as already discussed [14]. There is a relative good agreement between the predicted and measured quantities for the mixture $\{GR(SO_4^{2-}), Fe(OH)_2\}$. It is not the case for the three-compound mixture and this may be attributed to the existence of non-stoichiometric magnetite.

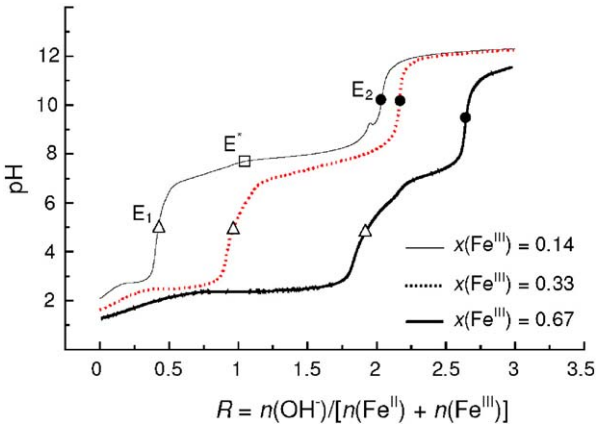

Fig. 3. Evolution of pH during the titration of different Fe^{II}–Fe^{III} solutions.

Fig. 3. Variation du pH au cours de la titration de différentes solutions mixtes Fe^{II}–Fe^{III}.

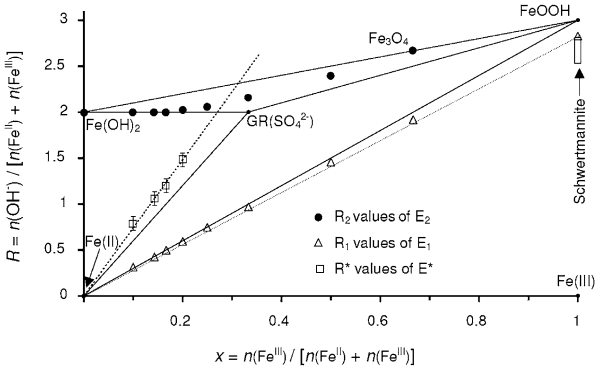

Fig. 4. R values of equivalent points E_1 and E_2 and point E^* presented in the mass-balance diagram.

Fig. 4. Valeurs de R pour les différents points E_1, E_2 et E^*, qui sont représentées dans le diagramme bilan matière.

The most interesting part of this analysis is the position of points E^* observed on the pH curves when $x \leqslant 0.2$ (Fig. 3). The pH values of the flat part of the second pH plateau, i.e. when $R^* < R < 2$, is very close to those measured during the titration of a standard Fe^{II} solution (not shown). It is therefore natural to propose that the first step of the second pH plateau, i.e. when $R < R^*$, corresponds to the full transformation of the initially formed ferric oxyhydroxide into $GR(SO_4^{2-})$. In the second step, i.e. when $R^* < R < 2$, the precipitation of the excess of Fe^{II}_{aq} present in solution leads to the formation of $Fe(OH)_2$. The (x, R^*) of points E^* presented in the mass-balance diagram in Fig. 4 increases roughly linearly according to $R^* = \alpha x$ where

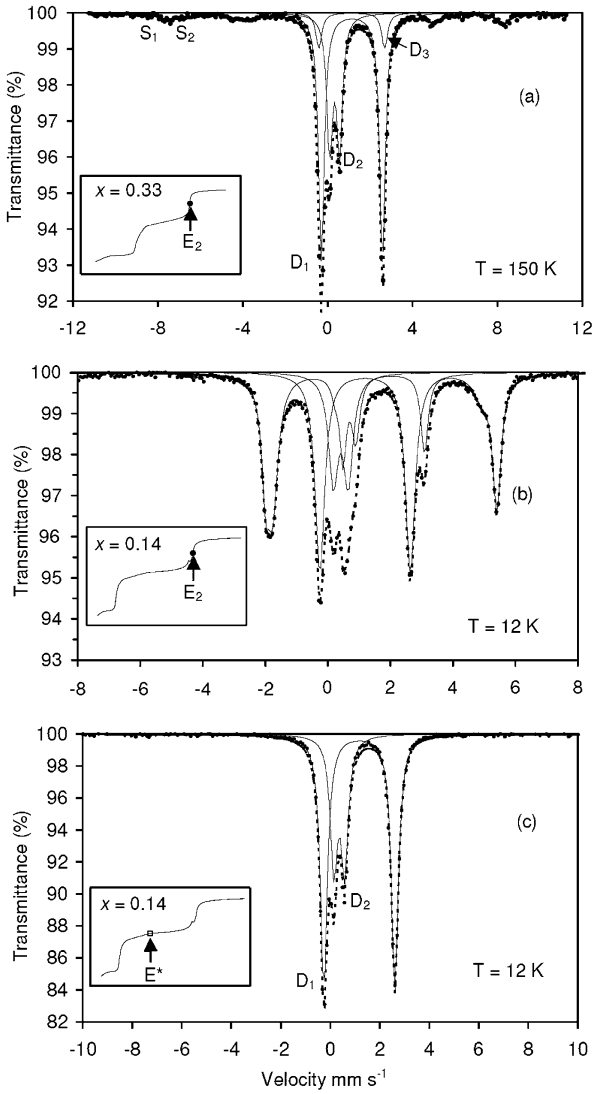

Fig. 5. Mössbauer spectra of the solid compounds obtained at different points of the titration curves.

Fig. 5. Spectres Mössbauer des composés solides obtenus en différents points des courbes de titration.

$\alpha = 7 \pm \sim 0.5$. This last linear relation is equivalent to a molar ratio $n(OH^-)/n(Fe^{III}) = 7 \pm \sim 0.5$. In a previous work [16], it was demonstrated with Mössbauer spectroscopy that $GR(SO_4^{2-})$ forms in the absence of any others solid compounds when exactly 7 moles of OH^- per mole of Fe^{III} were added. When $x = 0.14$, the Mössbauer spectrum of the sample obtained in these conditions contains only one ferrous doublet D_1 and one ferric doublet D_2 (Fig. 5c). The measured ratio $RA(D_1)/RA(D_2) = 1.94$ is in good agreement with the chemical formula $Fe^{II}{}_4Fe^{III}{}_2(OH)_{12}SO_4 \cdot \sim 8\,H_2O$. The fact that $GR(SO_4^{2-})$ forms when an excess of OH^- species is added is in apparent contradiction with what is expected if one considers the previous chemical formula where the ratio $n(OH^-)/n(Fe^{III})$ is equal to 6. This means that a certain amount OH^- species are consumed by another process that is concomitant to the formation of $GR(SO_4^{2-})$. Another important experimental evidence that such a process occurs is the fact that the value $R_2 = 2.16$ observed for the second equivalent point of the pH titration curves of the 'stoichiometric' solution, i.e. when $x = 0.33$, overshoots clearly the expected value $R = 2$ (Fig. 3). It can be seen on the same figure that such a phenomenon does not occur when $x = 0.67$ and the measured value $R_2 = 2.67$ is in very good agreement with the value expected for the formation of stoichiometric magnetite.

4.2. Analyses of Fe and SO_4^{2-} in aqueous solution

The different steps of the coprecipitation experiments were analysed by measuring the concentrations of Fe, Fe^{II} and SO_4^{2-} that remain in the aqueous medium during the titration of the $x = 0.33$ solution (Fig. 6). The grey dilution curve presented in Fig. 6a corresponds to the expected SO_4^{2-} concentration assuming that these anions are not incorporated in any precipitates. In this case, the variation of concentration is only due to the increase of volume corresponding to the addition of the NaOH solution. Calculated concentration curves were done by using the following hypotheses: (*i*) a ferric oxyhydroxide FeOOH precipitates during the first pH plateau by consuming 3 mol of OH^- per mole of Fe^{III} and the reaction is therefore finished at point B of abscissa $R = 1$; (*ii*) FeOOH reacts with $Fe^{II}{}_{aq}$ to form $GR(SO_4^{2-})$ by consuming 2 mol of OH^- per mole of iron and the reaction is accomplished at point C of abscissa $R = 2$; (*iii*) $GR(SO_4^{2-})$, which is unstable at pH $\sim$ 12 [16], is fully transformed into a mixture $\{Fe_3O_4, Fe(OH)_2\}$ at the end of the titration curve ($R = 3$).

The concentration of SO_4^{2-} anions measured in solution ($[SO_4^{2-}]_{exp}$) is clearly situated under the calculated curve between points A and B of Fig. 6a. This represents an experimental proof of the formation of a ferric sulphated basic salt, which begins when the flat part of the first pH plateau is reached. The decrease of the $[SO_4^{2-}]_{exp}$ values is followed by an increase at $R \sim 0.8$ and the experimental values reach again the calculated values around point B. This means that the initially formed ferric basic salt transforms into a ferric oxyhydroxide by releasing SO_4^{2-} anions in solution around equivalent point E_1. As expected, the $[SO_4^{2-}]_{exp}$ values decrease during the formation of $GR(SO_4^{2-})$ between

Table 2
Hyperfine parameters of the Mössbauer spectra presented in Fig. 5
Tableau 2
Paramètres hyperfins des spectres Mössbauer présentés sur la Fig. 5

Spectra	Compounds		δ	Δ or 2ε	H	*FWHM*	*RA* (%) measured	*RA* (%) predicted[a]
Fig. 5a	$GR(SO_4^{2-})$	D_1	1.29	2.87	—	0.32	53	$(D_1 + D_2)$ 52
		D_2	0.48	0.46	—	0.32	28	
	$Fe(OH)_2$	D_3	1.28	3.09	—	0.32	8	24
	Fe_3O_4	S_1	0.46	0	493	0.79	7	$(S_1 + S_2)$ 24
		S_2	0.86	0	468	0.69	4	
Fig. 5b	$GR(SO_4^{2-})$	D_1	1.32	2.88	—	0.37	34	$(D_1 + D_2)$ 43
		D_2	0.55	0.47	—	0.37	18	
	$Fe(OH)_2$[b]		1.3	−3.1	166	0.34	48	57
Fig. 5c	$GR(SO_4^{2-})$	D_1	1.32	2.86	—	0.34	66	$(D_1 + D_2)$
		D_2	0.52	0.43	—	0.34	34	100

δ (mm s^{-1}) isomer shift with respect to metallic α-iron at room temperature; Δ or 2ε (mm s^{-1}) quadrupole splitting; H (kOe) hyperfine field; *FWHM* (mm s^{-1}) full widths at half maximum; *RA* (%) relative abundance.
δ (mm s^{-1}) déplacement isomérique calculé en prenant le fer α à température ambiante comme référence ; Δ or 2ε (mm s^{-1}) éclatement quadripolaire ; H (kOe) champ hyperfin, *FWHM* (mm s^{-1}) largeur à mi-hauteur ; *RA* (%) abondance relative.
[a] Predicted by using the lever rules in the mass-balance diagram.
Valeurs prédites en utilisant la règle des leviers dans le diagramme bilan matière.
[b] Simulation of this component by a mixture of quantum states according to Génin [6].
Simulation de cette composante à l'aide d'un mélange d'état quantique d'après Génin [6].

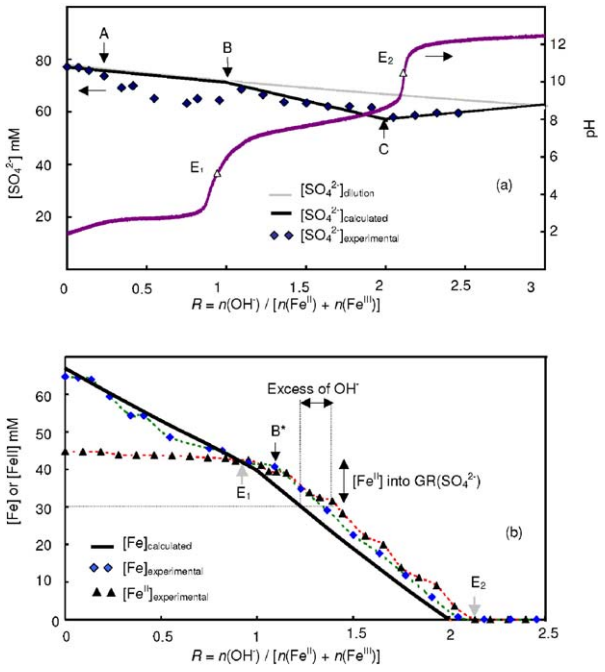

Fig. 6. Evolution of the concentrations $[SO_4^{2-}]$, [Fe] and $[Fe^{II}]$ in solution during the titration of the solution prepared for a ferric molar fraction $x = 0.33$.

Fig. 6. Variation des concentrations en solution $[SO_4^{2-}]$, [Fe] and $[Fe^{II}]$ pour la titration correspondant à une valeur $x = 0.33$ de la fraction molaire en ions Fe^{III}.

points E_1 and E_2 and then increase when $GR(SO_4^{2-})$ transforms into the mixture $\{Fe_3O_4, Fe(OH)_2\}$.

The Fe concentrations measured in solution ($[Fe]_{exp}$) are also situated slightly above the calculated values between points A and B confirming the formation of the ferric basic salt (Fig. 6b). By using both values $[SO_4^{2-}]_{exp}$ and $[Fe]_{exp}$ measured during the titration of the reference Fe^{III} solution ($x = 1$), the molar ratio $n(SO_4^{2-})/n(Fe^{III})$ of the ferric basic salt was calculated and it decreases between ~0.6 to 0.3 for increasing values of R ($1.25 \leqslant R \leqslant 2.27$). The evolution of the $[Fe]_{exp}$ values between points E_1 and E_2 is very interesting because the breakdown of the curves occurs at point B^*, situated at $R \sim 1.15$ (Fig. 6b). Then, the experimental curve decreases at a similar rate than the calculated curves, but stays always shifted to the right. As presented in Fig. 6b, this means that it is necessary to introduce an excess of OH^- in solution in order to precipitate a given amount of Fe^{II} into $GR(SO_4^{2-})$. This experimental result was confirmed by measuring the concentrations of Fe^{II} in solution. Between points E_1 and E_2, the curves corresponding to both $[Fe]_{exp}$ and $[Fe^{II}]_{exp}$ follow the same trends and are more or less superposed. Therefore, the concentration of Fe^{III} cations present in the aqueous solution when $GR(SO_4^{2-})$ forms is negligible.

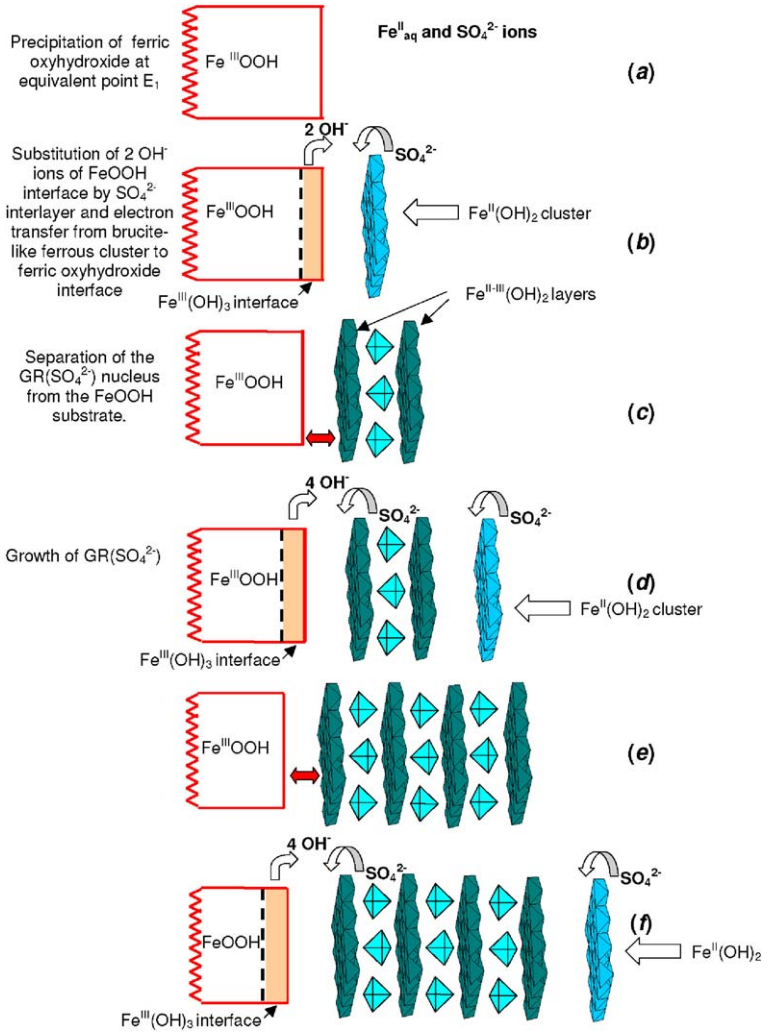

Fig. 7. Mode of formation of hydroxysulphate green rust $GR(SO_4^{2-})$. For the description of the different steps (a, b, c, ...) see the text.

Fig. 7. Mode de formation de la rouille verte sulfatée. La description des différentes étapes (a, b, c, ...) sont décrites dans le texte.

4.3. *Mode of formation of $GR(SO_4^{2-})$*

Analyses of the pH titration curves performed with the mass-balance diagram, Mössbauer spectroscopy and measurements of Fe and SO_4^{2-} concentrations in solution show that an excess of OH^- species is consumed while $GR(SO_4^{2-})$, i.e. $[Fe^{II}_4Fe^{III}_2(OH)_{12}]^{2+}\cdot[SO_4^{2-}\cdot\sim 8\,H_2O]$, is forming. This excess corresponds to an $n(OH^-)/n(Fe^{III})$ ratio of 7 instead of 6. It can be noticed that this amount corresponds also to the formation of the hypothetical mixture $[FeOOH + 2\,Fe(OH)_2]$, which would contain no sulphate. In fact, once point E_1 of the titration curves is reached, $Fe(OH)_2$ does not form but the surface of the initially formed FeOOH solid acts as a hydroxylating ligand towards Fe^{II} ions in solution. Therefore, the mechanism of formation of $GR(SO_4^{2-})$ more likely involves a surface reaction between the ferric oxyhydroxide and octahedrally co-ordinated Fe^{II} cations. At pH $\sim$ 5 (point E_1), partially hydroxylated ferrous species adsorbs on the FeOOH surface. At pH > 6–7, hydroxylation proceeds further and the formation of brucite like clusters by olation of $[Fe(OH)_2(OH_2)_4]^0$ complexes occurs [10,11]. As presented in Fig. 7, previously adsorbed SO_4^{2-} (or SO_4^{2-} anions coming from the solution) can get into the gap between the brucite like cluster and the FeOOH surface (Fig. 7b). This helps electrons to transfer from the ferrous cluster to the ferric interface through the interlayer. The hydroxylated solid-solution interface of bulk FeOOH can be consider as an $Fe^{III}(OH)_3$ layer and therefore the chemical reaction can

be written as follows:

$$4\,[Fe^{II}(OH)_2]_{cluster} + 2\,Fe^{III}(OH)_{3interface} + SO_4{}^{2-} \Leftrightarrow [Fe^{II}{}_4Fe^{III}{}_2(OH)_{12}SO_4] + 2[OH^-]_{excess}$$

The interlayer of $SO_4{}^{2-}$ anions between two brucite-like $Fe^{II-III}(OH)_2$ layers is electrostatically balanced and an excess of OH^- ion is released; a $Fe^{II-III}(OH)_2$ cluster is now separated from the bulk substrate (Fig. 7c). Lateral growth of the clusters in the [100] direction proceeds much faster than in the [001] direction in order to obtain the flat hexagonal plates observed with TEM (Fig. 12). The process can be repeated if a new $Fe^{II}(OH)_2$ cluster forms on the top of this first $GR_2(SO_4{}^{2-})$ nucleus (Fig. 7d). Two $SO_4{}^{2-}$ interlayers may form simultaneously and the electron transfer is again accomplished from the Fe^{II} donor within the brucite-like cluster towards the Fe^{III} acceptor of the oxyhydroxide interface (Fig. 7e). Therefore, it seems inappropriate to qualify the process as dissolution–reprecipitation. The $GR_2(SO_4{}^{2-})$ crystal grows in situ at the expense of the FeOOH substrate by electron transfer.

5. Chemical composition of green rust

5.1. Hydroxysulphate green rust $Fe^{II}{}_4Fe^{III}{}_2(OH)_{12}SO_4{\cdot}{\sim}8H_2O$

Fe^{II}–Fe^{III} solutions were precipitated by a NaOH solution at a constant ratio $R = n(OH^-)/n(Fe) = 2$, as presented in Table 1. The Mössbauer spectra and hyperfine parameters obtained for three different values of the ferric molar fraction x are presented in Fig. 8 and Table 3, respectively. It appears that $GR(SO_4{}^{2-})$ precipitates in the quasi-absence of any other compound only when $x = 0.33$ (Fig. 8b). Nevertheless, traces of Fe_3O_4 and/or FeOOH that correspond to a very low intensity sextet are present. When $x = 0.28$, the sample is a mixture of two compounds, i.e. $\{GR(SO_4{}^{2-}), Fe(OH)_2\}$, and a mixture of three compound when $x = 0.46$, i.e. $\{GR(SO_4{}^{2-}), Fe_3O_4, FeOOH\}$. Whatever the sample is, a Fe^{II}:Fe^{III} ratio of ∼1:2 is measured by using the relative areas of doublets D_1 and D_2 of $GR(SO_4{}^{2-})$. Therefore, $GR(SO_4{}^{2-})$ has a well-defined stoichiometry that corresponds to the normalised chemical formula $[Fe^{II}{}_{0.67}Fe^{III}{}_{0.33}(OH)_2]^{0.33+}{\cdot}[(0.165)\,SO_4{\cdot}{\sim}(1.33)\,H_2O]^{0.33-}$.

5.2. Hydroxycarbonate green rust

Fe^{II}–Fe^{III} solutions were precipitated by a Na_2CO_3 solution at a constant molar ratio $R = n(CO_3{}^{2-})/n(Fe) = 2.5$, as presented in Table 1. The samples were filtered and analysed immediately after the synthesis in order to avoid the transformation of $GR(CO_3{}^{2-})$ in a mixture of magnetite and siderite. On the contrary to what was observed for $GR(SO_4{}^{2-})$, typical spectra of $GR(CO_3{}^{2-})$ that contain three doublets were obtained for both values $x = 0.25$ and $x = 0.33$ (Fig. 9a and b and Table 4). As predicted by using structural models [7],

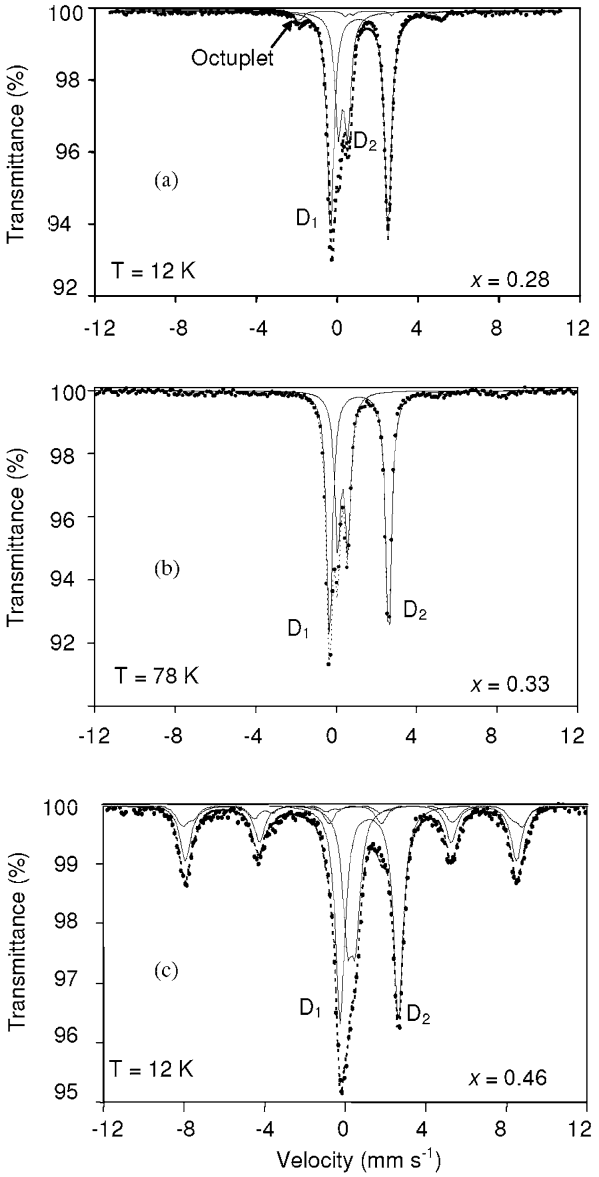

Fig. 8. Evolution of the Mössbauer spectra as a function of the ferric molar fraction x for samples prepared in a sulphated aqueous medium at a constant hydroxylation level $R = 2$.

Fig. 8. Évolution des spectres Mössbauer en fonction de la fraction molaire en ions Fe^{III} pour des échantillons préparés à un taux d'hydroxylation constant $R = 2$.

Table 3
Hyperfine parameters of the Mössbauer spectra presented in Fig. 8
Tableau 3
Paramètres hyperfins des spectres Mössbauer présentés sur la Fig. 8

Spectra	Compounds		δ	Δ or 2ε	H	$FWHM$	RA (%)
Fig. 8a	$GR(SO_4^{2-})$	D_1	1.32	2.88	—	0.37	63.5
		D_2	0.55	0.47	—	0.37	32
	$Fe(OH)_2$		1.3	−3.1	166	0.34	4.5
Fig. 8b	$GR(SO_4^{2-})$	D_1	1.35	2.88	—	0.37	60
		D_2	0.49	0.5	—	0.37	35
		S	0.69	0	474	0.34	5
Fig. 8c	$GR(SO_4^{2-})$	D_1	1.32	2.86	—	0.55	40
		D_2	0.52	0.43	—	0.55	22
		S_1	0.46	0	529	0.63	4
	Fe_3O_4	S_2	0.5	0	519	0.55	5
		S_3	0.79	−0.59	490	0.55	5
	FeOOH	S_4	0.5	−0.23	510	0.71	24

δ (mm s^{-1}) isomer shift with respect to metallic α-iron at room temperature; Δ or 2ε (mm s^{-1}) quadrupole splitting; H (kOe) hyperfine field; $FWHM$ (mm s^{-1}) full widths at half maximum; RA (%) relative abundance.
δ (mm s^{-1}) déplacement isomérique calculé en prenant le fer α à température ambiante comme référence ; Δ ou 2ε (mm s^{-1}) éclatement quadripolaire ; H (kOe) champ hyperfin, $FWHM$ (mm s^{-1}) largeur à mi-hauteur ; RA (%) abondance relative.

the area ratio between doublets D_1:D_2:D_3 is close to 1/2:1/3:1/6 for the sample prepared at $x = 0.33$. Doublet D_3 was attributed to Fe^{II} species that has CO_3^{2-} anions in their neighbourhood and a decrease of the relative area of doublet D_3 is effectively observed for the green rust sample that contains less carbonate anions, i.e. when $x = 0.25$ (Fig. 8a).When $x = 0.4$, the Mössbauer spectrum corresponds to a mixture of green rust and magnetite $\{GR(CO_3^{2-}), Fe_3O_4\}$ and the Fe^{II}:Fe^{III} ratio of $GR(CO_3^{2-})$ is close to 2:1. The relative abundance of Fe_3O_4 that is given in Table 4, i.e. 23%, is in good agreement with the quantity predicted by using the lever rule in the mass-balance diagram, i.e. 21%. Finally, $GR(CO_3^{2-})$ has a variable chemical composition that corresponds to the normalised chemical formula $[Fe^{II}_{(1-x)}Fe^{III}_x(OH)_2]^{x+}\cdot[(x/n)\,CO_3^{2-}\cdot m\,H_2O]^{x-}$ where $\sim 0.25 < x < 0.33$.

5.3. Comparison with other layered double hydroxides

It has been often reported that most of the members of the M^{II}–M^{III} layered double hydroxides (LDH) family of general chemical composition $[M^{II}_{(1-x)}M^{III}_x(OH)_2]^{x+}\cdot[(x/n)A^{n-}\cdot mH_2O]^{x+}$ [13] have an upper limit of composition $x = 0.33$. This limit is generally attributed to the fact that if $x > 0.33$, M^{III} cations become nearest neighbours in the brucite-like layer and this is hardly possible due to electrostatic repulsion. If this last rule is respected for $x = 0.33$, the cation layer is characterised by an ordered array, where all M^{III} cations are surrounded by six M^{II} cations. It appears that green rusts obey the same rule than the other LDHs.

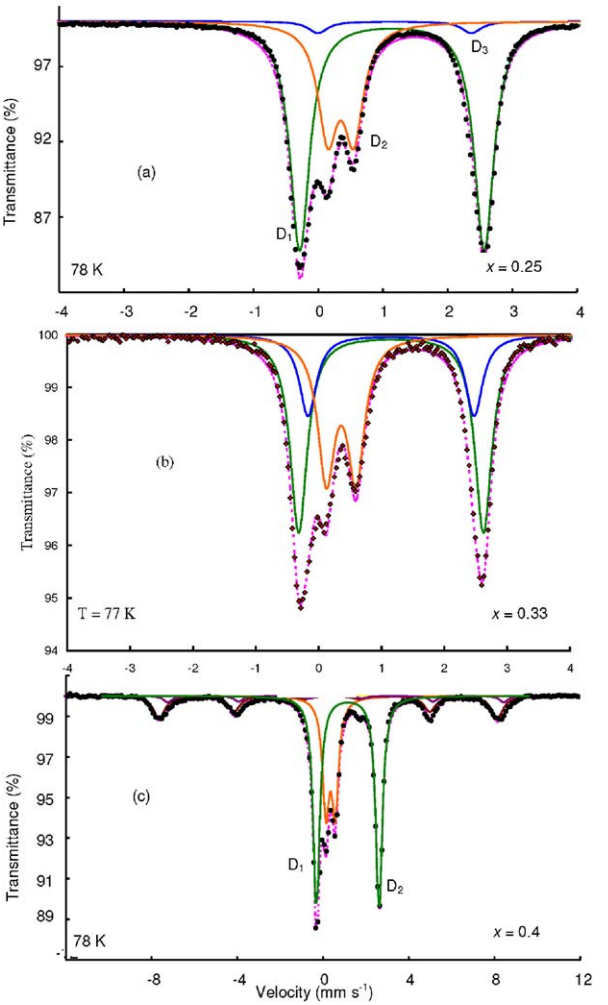

Fig. 9. Evolution of the Mössbauer spectra as a function of the ferric molar fraction x for samples prepared in a carbonated aqueous medium.

Fig. 9. Évolution des spectres Mössbauer en fonction de la fraction molaire en ions Fe^{III} pour des échantillons préparée en milieu carbonaté.

6. Synthesis of Al-substituted hydroxysulphate green rust and crystals morphology

Al-Substituted hydroxysulphate green rust {Al-$GR(SO_4^{2-})$} samples were prepared in excess of Fe^{II}, i.e. $x(Fe^{II}) = 0.8$, by adding a NaOH solution at a ratio $n(OH^-)/[n(Fe^{III}) + n(Al^{III})] = 7$. The chemical for-

Table 4
Hyperfine parameters of the Mössbauer spectra presented in Fig. 9
Tableau 4
Paramètres hyperfins des spectres Mössbauer présentés sur la Fig. 9

Spectra	Compounds		δ	Δ or 2ε	H	*FWHM*	*RA* (%)
Fig. 9a	GR(CO_3^{2-})	D_1	1.25	2.84	–	0.36	65
		D_2	0.48	0.39	–	0.36	28
		D_3	1.25	2.39	–	0.36	7
Fig. 9b	GR(CO_3^{2-})	D_1	1.28	2.87	–	0.34	48
		D_2	0.47	0.43	–	0.34	34
		S	1.28	2.55		0.34	19
Fig. 9c	GR(CO_3^{2-})	D_1	1.3	2.9	–	0.38	52
		D_2	0.5	0.47	–	0.38	25
	Fe_3O_4	S_1	0.43	0	490	0.63	17
		S_2	0.5	0	482	0.55	6

δ (mm s^{-1}) isomer shift with respect to metallic α-iron at room temperature; ΔE_Q or 2ε (mm s^{-1}) quadrupole splitting; H (kOe) hyperfine field; *FWHM* (mm s^{-1}) full widths at half maximum; *RA* (%) relative abundance.
δ (mm s^{-1}) déplacement isomérique calculé en prenant le fer α à température ambiante comme référence ; Δ or 2ε (mm s^{-1}) éclatement quadripolaire ; H (kOe) champ hyperfin, *FWHM* (mm s^{-1}) largeur à mi-hauteur ; *RA* (%) abondance relative.

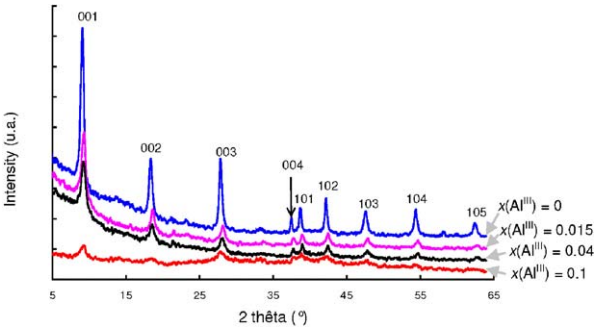

Fig. 10. XRD patterns of Al-substituted hydroxysulphate green rust samples that contain increasing amount of aluminium.

Fig. 10. Diffractogrammes de rayons X pour des échantillons de rouille verte sulfatée substituée aluminium.

mula of the expected compound is $[Fe^{II}_{0.67}Fe^{III}_{(0.33-y)}Al^{III}_{y}(OH)_2]^{0.33+} \cdot [(0.165)\,SO_4 \cdot 1.33\,H_2O]^{0.33-}$, with $0 \leqslant y \leqslant 0.33$. The substitution of Fe^{III} cations by Al^{III} cations is clearly demonstrated by using XRD and a progressive shift of the lines to higher angle is observed when the amount of Al^{III} increases (Fig. 10). This corresponds to lower cell parameters for Al-GR(SO_4^{2-}). When $y = 0.167$, the values $a = 0.318$ nm and $c = 1.095$ nm are measured for Al-GR(SO_4^{2-}) in comparison with $a = 0.321$ nm and $c = 1.104$ nm for GR(SO_4^{2-}). The cell parameters decrease because the ionic radius of Al^{III}, i.e. $r(Al^{III}) = 0.53$ Å, is lower than the ionic radius of Fe^{III}, i.e. $r(Fe^{III}) = 0.64$ Å.

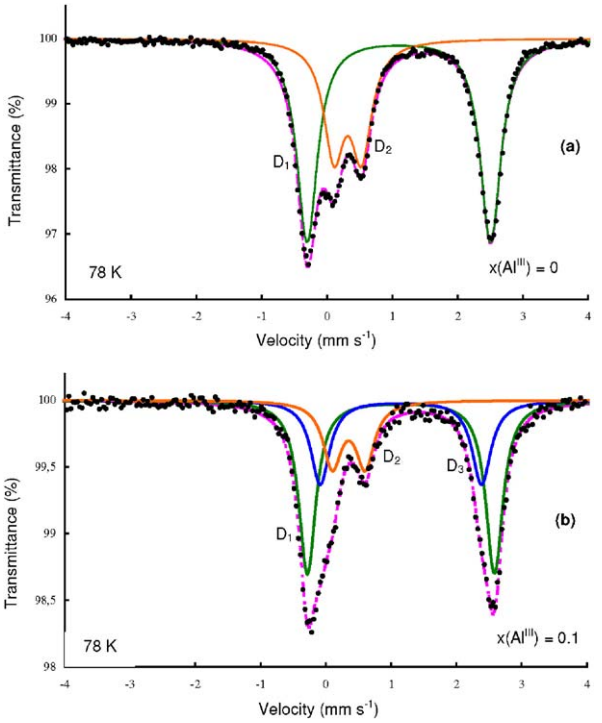

Fig. 11. Mössbauer spectra of hydroxysulphate green rust (**a**) and Al-substituted hydroxysulphate green rust (**b**).

Fig. 11. (**a**) Spectre Mössbauer de la rouille verte sulfatée, (**b**) spectre Mössbauer de la rouille verte sulfatée substituée.

Table 5
Hyperfine parameters of the Mössbauer spectra presented in Fig. 11
Tableau 5
Paramètres hyperfins des spectres Mössbauer présentés sur la Fig. 11

Spectra	Compounds		δ	Δ	*FWHM*	*RA* (%)
Fig. 11a	GR(SO_4^{2-})	D_1	1.27	2.80	0.35	65
		D_2	0.44	0.42	0.35	35
Fig. 11b	Al-GR(SO_4^{2-})	D_1	1.27	2.84	0.34	56
		D_2	0.47	0.49	0.34	20
		D_3	1.27	2.44	0.34	24

δ (mm s^{-1}) isomer shift with respect to metallic α-iron at room temperature; Δ (mm s^{-1}) quadrupole splitting; *FWHM* (mm s^{-1}) full widths at half maximum; *RA* (%) relative abundance.
δ (mm s^{-1}) déplacement isomérique calculé en prenant le fer α à température ambiante comme référence ; Δ (mm s^{-1}) éclatement quadripolaire ; *FWHM* (mm s^{-1}) largeur à mi-hauteur ; *RA* (%) abondance relative.

The Mössbauer spectrum of Al-GR(SO_4^{2-}) is characterised by the presence of a new ferrous doublet D_3 and an increase of the Fe^{II}:Fe^{III} ratio equal to 4:1 for the compound $[Fe^{II}_{0.67}Fe^{III}_{0.167}Al^{III}_{0.167}(OH)_2]^{0.33+} \cdot [(0.165)\,SO_4 \cdot 1.33\,H_2O]^{0.33-}$ (Fig. 11 and Table 5). As shown previously [1], the presence of two ferrous dou-

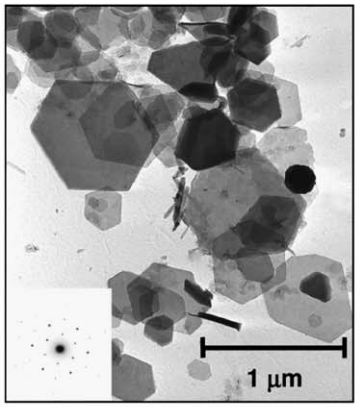

(a) GR(SO_4^{2-})

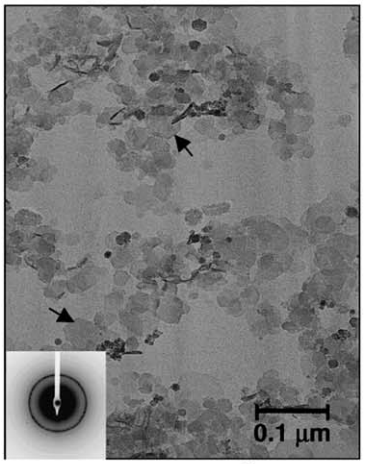

(b) Al-GR(SO_4^{2-})

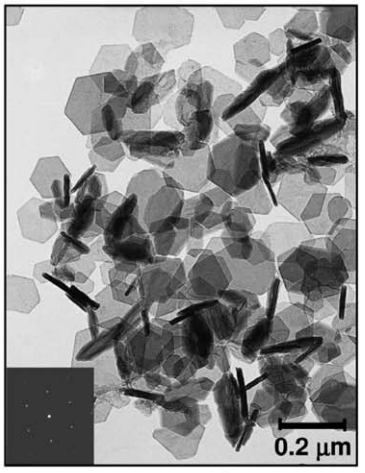

(c) GR(CO_3^{2-})

Fig. 12. TEM images of hydroxysulphate green rust (**a**), Al-substituted hydroxysulphate green rust (**b**) and hydroxycarbonate green rust (**c**).

Fig. 12. Images de microscopie électronique en transmission : (**a**) rouille verte sulfatée, (**b**) rouille verte sulfatée substituée aluminium, (**c**) rouille verte carbonatée.

blets is attributed to the fact that Fe^{II} cations have both Fe and Al atoms in their neighbourhood.

A gradual increase of the width of the XRD lines is also observed in Fig. 10. As expected, the size of the hexagonal crystals of Al-GR(SO_4^{2-}), i.e. ∼50 nm, is much lower than the crystal size of GR(SO_4^{2-}), i.e. ∼500 nm (Fig. 12a and b). In a previous study [5], it has been shown that GR(SO_4^{2-}) crystals are much flatter than GR(CO_3^{2-}) crystals. Therefore, several GR(CO_3^{2-}) crystals that stay roughly perpendicularly to the grid are observed in Fig. 12c.

7. Conclusion

The coprecipitation of Fe^{II} and Fe^{III} species was studied by using a mass-balance diagram. A direct visualisation of the nature and the relative quantities of the compounds that form is obtained by following simple geometrical rules. In sulphated aqueous medium, the formation of hydroxysulphate green rust {GR(SO_4^{2-})} is accompanied by the consumption of an excess of OH^- species if one considers the chemical formula $Fe^{II}_4Fe^{III}_2(OH)_{12}SO_4\cdot \sim 8\,H_2O$. A mechanism of formation is proposed, where adsorbed octahedrally coordinated Fe^{II} cations and SO_4^{2-} anions layers react at the surface of the ferric oxyhydroxide. GR(SO_4^{2-}) crystals grow in situ at the FeOOH/solution interface by electron transfer. Contrary to GR(SO_4^{2-}), GR(CO_3^{2-}) has a variable chemical composition, i.e. is $[Fe^{II}_{(1-x)}Fe^{III}_x(OH)_2]^{x+}\cdot[(x/n)CO_3^{2-}\cdot m\,H_2O]^{x+}$, where $\sim 0.25 < x < 0.33$. The coprecipitation method was also used to synthesise Al-substituted hydroxysulphate green rust {Al-GR(SO_4^{2-})}. Transmission electron microscopy images of green rust shows hexagonal plates and a decrease of crystal size in the order GR(SO_4^{2-}) > GR(CO_3^{2-}) > Al-GR(SO_4^{2-}). The use of the mass-balance diagram is not limited to the study of precipitation reactions and all the chemical reactions that occur in the redox cycle of iron can be visualised.

Acknowledgements

The authors would like to thank Prof. Jean-Pierre Jolivet (‘Université Pierre-et-Marie-Curie’, Paris, France) for fruitful discussion, Dr Jaafard Ghanbaja (‘Université Henri-Poincaré’, Nancy, France) for performing the TEM experiments and Dr Isabelle Bihannic (Laboratoire ‘Environnement Minéralurgie’, INPL, Nancy, France) for the XRD patterns of Al-substituted green rusts.

References

[1] R. Aissa, C. Ruby, A. Géhin, M. Abdelmoula, J.-M.R. Génin, Synthesis by coprecipitation of Al-substituted hydroxysulphate green rust $Fe^{II}_4Fe^{III}_2Al^{III}_y(OH)_{12}SO_4 \cdot n\,H_2O$, Hyperfine Interact. 156–157 (2004) 445–451.

[2] T.V. Arden, The solubility products of ferrous and ferrosic hydroxides, J. Chem. Soc. (1950) 882–885.

[3] O. Benali, M. Abdelmoula, P. Refait, J.-M.R. Génin, Effect of orthophosphate on the oxidation products of Fe(II)–Fe(III) hydroxycarbonate: the transformation of green rust to ferrihydrite, Geochim. Cosmochim. Acta 65 (2001) 1715–1726.

[4] J.M. Bigham, U. Schwertmann, L. Carlson, E. Murad, A poorly crystallized oxyhydroxysulfate of iron formed by bacterial oxidation of iron(II) in acid mine waters, Geochim. Cosmochim. Acta 54 (1990) 2743–2758.

[5] F. Bocher, A. Géhin, C. Ruby, J. Ghanbaja, M. Abdelmoula, J.-M.R. Génin, Coprecipitation of Fe(II–III) hydroxycarbonate green rust stabilised by phosphate adsorption, Solid-State Sci. 6 (2004) 117–124.

[6] J.-M.R. Génin, P. Bauer, A.A. Olowe, D. Rézel, Mössbauer study of the kinetics of simulated corrosion process of iron in chlorinated aqueous solution around room temperature: the hyperfine structure of ferrous hydroxides and green rust I, Hyperfine Interact. 29 (1986) 1355–1360.

[7] J.-M.R. Génin, C. Ruby, Anion and cation distributions in Fe(II–III) hydroxysalt green rusts from XRD and Mössbauer analysis (carbonate, chloride, sulphate...); the 'fougerite' mineral, Solid-State Sci. 6 (2004) 705–718.

[8] H.C.B. Hansen, Composition, stabilization, and light absorption of iron(II)–iron(III) hydroxycarbonate ('Green rust'), Clay Miner. 24 (1989) 663–669.

[9] J.-P. Jolivet, P. Belleville, E. Tronc, J. Livage, Influence of iron(II) on the formation of the spinel iron oxide in alkaline medium, Clays Clay Miner. 40 (1992) 531–539.

[10] J.-P. Jolivet, in: Metal Oxide Chemistry and Synthesis, From Solution to Solid State, Wiley, Chichester, UK, 2000, pp. 288–300.

[11] J.-P. Jolivet, C. Chanéac, E. Tronc, Iron oxide chemistry, from molecular clusters to extended solid networks, Chem. Commun. (2004) 481–487.

[12] S. Mann, N.H.C. Sparks, S.B. Couling, M.C. Larcombe, R.B. Frankel, Crystallochemical characterization of magnetic spinels prepared from aqueous solution, J. Chem. Soc. Faraday Trans. 1 85 (1989) 3033–3044.

[13] A. de Roy, C. Forano, J.-P. Besse, in: V. Rives (Ed.), Synthesis and Post-Synthesis Modifications in Layered Double Hydroxides, Nova Science Publishers, 2001, pp. 1–37.

[14] C. Ruby, A. Géhin, M. Abdelmoula, J.-M.R. Génin, J.-P. Jolivet, Coprecipitation of Fe(II) and Fe(III) cations in sulphated aqueous medium and formation of hydroxysulphate green rust, Solid-State Sci. 5 (2004) 1055–1062.

[15] Y.T. Tamaura, K. Ito, T. Katsura, Transformation of γ-FeOOH to Fe_3O_4 by adsorption of iron (II) ion on γ-FeOOH, J. Chem. Soc. Dalton Trans. (1983) 189–194.

[16] R.M. Taylor, Formation and properties of iron(II)iron(III) hydroxycarbonate and its possible significance in soil formation, Clay Miner. 15 (1980) 369–382.

[17] E. Tronc, P. Belleville, J.-P. Jolivet, J. Livage, Transformation of ferric hydroxide into spinel by iron(II) adsorption, Langmuir 8 (1992) 313–319.